Calcium isotope fractionation during microbially induced carbonate mineral precipitation

Harold J. Bradbury[1,*,#], Kathryn H. Halloran[1,2,#], Chin Yik Lin[1,3], Alexandra V. Turchyn[1]

[1] Department of Earth Sciences, University of Cambridge, Cambridge, UK.

[2] Department of Geology, Faculty of Science, University of Malaya, 50603, Kuala Lumpur, Malaysia.

[3] Department of Marine Chemistry & Geochemistry, Woods Hole Oceanographic Institution, Woods Hole, MA 02543, USA.

[*]Corresponding author: hjb62@cam.ac.uk

[#]These authors contributed equally to this work

Keywords: calcium isotope fractionation; sulfate reducing bacteria; carbonate precipitation.

Abstract

We report the calcium isotope fractionation during the microbially-induced precipitation of calcium carbonate minerals in pure cultures of the marine sulfate-reducing bacterium *Desulfovibrio bizertensis*. These data are used to explore how the calcium isotope fractionation factor during microbially-induced carbonate mineral precipitation differs from the better-constrained calcium isotope fractionation factors during biogenic or abiotic carbonate mineral precipitation. Bacterial growth was then modulated with antibiotics, and the evolution of $\delta^{44}Ca$ in solution was monitored under different microbial growth rates. The faster the microbial growth rate, the larger the calcium isotope fractionation during carbonate mineral precipitation, ranging from $\Delta^{44}Ca_{(s\text{-}f)}$ between -1.07‰ and -0.48‰. The reported calcium isotope fractionation can help us understand the link between calcium isotope fractionation and microbial metabolism in carbonate minerals precipitated during sedimentary diagenesis.

1. Introduction

Reconstructing the carbon cycle over Earth history has long been approached through analysis of the carbon isotope composition of carbonate minerals and rocks (Garrels and Lerman, 1981; Berner et al., 1983; Kump and Arthur, 1999; Berner, 2003). Recently, there have been increasing numbers of studies reporting the calcium isotopic composition (reported in delta notation as a ratio of ^{44}Ca to ^{40}Ca as $\delta^{44}Ca$) of carbonate minerals and rocks as an additional tool for exploring the past carbon and calcium cycles (Skulan et al., 1997; Zhu and Macdougall, 1998; De La Rocha and DePaolo, 2000; Fantle and DePaolo, 2005; Fantle and Tipper, 2014; Farkaš et al., 2016). When the analysis of calcium isotopes in carbonate minerals are paired with the standard measurement of carbon isotope ratios in carbonate minerals, reconstruction of the various fluxes in the carbon cycle can be accomplished as well as far better constraints can be placed on the influence of diagenesis, or post depositional recrystallisation, on the geological record (Higgins et al., 2018; Ahm et al., 2018).

Carbonate rocks contain original carbonate minerals that precipitate in the water column or at the sediment water-interface, either biogenically or, in unique cases, abiotically. These carbonate minerals may have undergone dissolution or diagenetic alteration during early or late stage diagenesis, when less stable carbonate polymorphs transform to more stable carbonate polymorphs (Milliman, 1993; Higgins et al., 2018). In addition, carbonate rocks contain sedimentary-precipitated carbonate mineral cements, which can help to 'glue' the rock together. The environmental conditions under which primary carbonate minerals precipitate is typically different to those under which sedimentary carbonate minerals precipitate, although it has recently been shown that very early precipitation of diagenetic calcite can record original carbon isotope signals (Kozdon et al., 2018). These differing environmental conditions can influence the carbon and calcium isotopic composition of carbonate minerals, and therefore carbonate rocks (Lau et al., 2017; Higgins et al., 2018). Sedimentary (also termed authigenic) carbonate mineral precipitation is often driven by microbially-induced chemical changes in sedimentary pore fluids, where through anaerobic microbial metabolism, there is an increase in dissolved inorganic carbon driving supersaturated conditions in the subsurface (Hein et al., 1979; Lein, 2004; Teichert et al., 2009; Schrag et al., 2013). Thus, the calcium (and carbon) isotopic composition of a

bulk carbonate rock may reflect both the calcium isotopic composition of the primary minerals and that of the sedimentary cement.

Calcium has two dominant isotopes, ^{40}Ca and the less abundant ^{44}Ca. Calcium carbonate mineral precipitation preferentially takes the lighter ^{40}Ca isotope, leaving the heavy ^{44}Ca isotope behind, resulting in calcium carbonate minerals with a low $\delta^{44}Ca$ and the fluid from which they precipitate with an increasingly higher $\delta^{44}Ca$ (Zhu and Macdougall, 1998). At calcium isotopic equilibrium, the difference between the calcium isotopic composition of the fluid ($\delta^{44}Ca_{(aq)}$) and that of the mineral ($\delta^{44}Ca_{(carbonate)}$), often reported as $\Delta^{44}Ca_{(carb\text{-}aq),}$ is understood to be 0‰ based on modeling of deep-sea pore fluids (Fantle and DePaolo, 2007; Fantle, 2015; Huber et al., 2017). Very few minerals precipitate in calcium isotopic equilibrium with the fluid from which they derive, and a kinetic calcium isotope fractionation results in the preferential partitioning of ^{40}Ca into the mineral phase when carbonate minerals precipitate (Gussone et al., 2005; Teichert et al., 2009). Experimental studies have explored variability in the magnitude of this kinetic calcium isotope fractionation based on both the type of $CaCO_3$ precipitating and on physical and chemical properties of the solution like temperature, pH, and ion concentration, all of which are ultimately related to the rate of mineral precipitation. This rate of calcium carbonate precipitation is believed to exert the dominant control on calcium isotope fractionation during mineral formation, which varies between the 0‰ equilibrium and ~2‰ (Gussone et al., 2003; Gussone et al., 2005; Tang et al., 2008a; DePaolo, 2011; Nielsen et al., 2012; AlKhatib and Eisenhauer, 2017b). This range of magnitudes of calcium isotope fractionation has limited the use of calcium isotopes as a direct proxy for paleoceanography, as changes in the $\delta^{44}Ca$ of any mineral phase can reflect changes in the dominant mineralogy (Husson et al., 2015; Jost et al., 2017; Lau et al., 2017), changes in the rate of mineral precipitation (Tang et al., 2008a; Du Vivier et al., 2015; AlKhatib and Eisenhauer, 2017b; AlKhatib and Eisenhauer, 2017a; Linzmeier et al., 2019), and changes in the degree of fluid vs. sediment-buffering during carbonate diagenesis (Higgins et al., 2018; Ahm et al., 2018; Ahm et al., 2019). Indeed, many studies have concluded that $\delta^{44}Ca$ in the geological record is best used as a diagnostic tool for diagenesis (Lau et al., 2017; Higgins et al., 2018; Ahm et al., 2019).

Within the sediment column there are two main processes which impact the calcium isotope composition of the pore fluid, authigenic carbonate precipitation and recrystallisation. In theory, authigenic carbonate precipitation should preferentially remove the lighter ^{40}Ca from the fluid, driving the pore fluid $\delta^{44}Ca$ to increasing values, although initial studies saw little evidence of this (Teichert et al., 2009). Recrystallisation involves the exchange of calcium between the fluid and solid phase, and causes the $\delta^{44}Ca$ of the pore fluid to approach solid values (Fantle and DePaolo, 2007; Fantle, 2015; Huber et al., 2017). Recent work has also demonstrated that calcium isotopes can be used to observe both increases in $\delta^{44}Ca$ in the pore fluid caused by authigenic carbonate precipitation and decreases in $\delta^{44}Ca$ in the pore fluid caused by recrystallisation in the same site (Bradbury and Turchyn, 2018).

While there have been many studies of the calcium isotope fractionation during abiotic and biogenic carbonate mineral precipitation, these studies may or may not translate to microbially-induced carbonate mineral precipitation. When microbes induce the precipitation of carbonate minerals there may be different controls on the calcium isotope fractionation due to the presence of extracellular polymeric substances (EPS), different mechanisms of mineral growth, or unique micro-scale chemical environments generated by microbes (Aloisi et al., 2006; Krause et al., 2012; Krause et al., 2018). Thus, bridging the gap between the experimental and modeling studies of calcium isotope fractionation during microbially-induced carbonate precipitation and what is actually measured in a carbonate rock or carbonate sediment remains challenging.

Several previous studies have attempted to understand calcium isotope fractionation during microbially induced carbonate precipitation in the environment, which are summarized in Table 1. In one study, bacterial sulfate reduction in clogged well bores was stimulated with the addition of acetate. In well bores where a decrease in the concentration of aqueous calcium was observed, there was an accompanying increase in $\delta^{44}Ca$ of the well fluid ranging from 1-2.5‰, with a calculated calcium isotope fractionation of -1‰ (Druhan et al., 2013). In another study, authigenic aragonite from a cold seep on the Cascadia margin off the Oregon coast had a $\delta^{44}Ca$ range from -0.56 to +0.18‰, with a fluid $\delta^{44}Ca$ ranging from 1.3-2.0‰ (Teichert et al., 2005). In these aragonite samples, mineral layers further from the presumed nucleus of precipitation

are enriched in ^{44}Ca, which was explained by the progressive enrichment of ^{44}Ca in pore water fluid as ^{40}Ca preferentially incorporates into the solid, aragonite, phase. The authors calculated a calcium isotope fractionation factor during authigenic aragonite precipitation of $\alpha = 0.99813$ at 4.7 ˚C, meaning aragonite is 1.9‰ lower than the fluid from which it precipitated, assuming there was a 30% decrease in calcium concentration (Teichert et al., 2005). Additional work at a different cold methane seep in the Niger delta region identified carbonate minerals with a $\delta^{44}Ca$ of -0.5-0.5‰, with an accompanying pore fluid $\delta^{44}Ca$ of 0.5-1.9‰, with a solid-to-fluid offset of up to -1.4‰ (Henderson et al., 2006). Finally, carbonate minerals precipitating from cold seeps in the South China Sea were found to be dominated by dolomite, calcite, and aragonite, with a $\delta^{44}Ca$ range from 0.21 to 0.55‰, and a solid to fluid offset of -0.67 to -0.36‰ (Wang et al., 2012). In this case, the high $\delta^{44}Ca$ in the measured mineral samples was attributed to either fast rates of mineral precipitation or to an aqueous pool of calcium enriched in ^{44}Ca due to Rayleigh fractionation-type processes. In these studies in the natural environment of microbially induced carbonate mineral precipitation, the solid to fluid offset ranged between -1.9‰ to -0.36‰. This range comes with the caveat that there were few constraints on the microbial populations involved in inducing mineral precipitation but demonstrates the challenges associated with calculating absolute calcium isotope fractionation factors in natural systems.

Table 1: Calculated $\Delta^{44}Ca_{(s\text{-}f)}$ from studies in both natural systems (1-4) and pure cultures (5-6).

Study	$\Delta^{44}Ca_{(s\text{-}f)}$	Temperature
Druhan et al., 2013	-1±0.5‰	15°C
Teichert et al., 2005	-1.9‰	4.7°C
Henderson et al., 2006	-1.4‰	Unreported
Wang et al., 2012	-0.67 to -0.36‰	Unreported
Krause et al. 2012	-1.10±0.24‰	21°C
Krause et al. 2018	-1.19±0.22‰	20°C

In contrast, other studies have used pure cultures of bacteria to directly examine the calcium isotope fractionation during microbially induced calcium carbonate mineral precipitation. Pure cultures of the sulfate-reducing bacterium *Desulfobulbus mediterraneus*, were measured, showing progressive enrichment in ^{40}Ca from culture

media to biological material to the carbonate minerals precipitated (Krause et al., 2012). Calcium isotope ratios were measured in the initial and final culture media (final $\delta^{44}Ca$ = 1.1 ± 0.24‰), extracellular polymeric substances (EPS) with cell material ($\delta^{44}Ca$ = 0.48 ± 0.11‰), and precipitated dolomite ($\delta^{44}Ca$ = 0.05 ± 0.24‰). It was concluded that there was a two-step calcium isotope fractionation, with calcium isotope fractionation during the initial association of calcium with the bacterial biofilm, and further calcium isotope fractionation with the precipitation of dolomite (Krause et al., 2012). In their study it was suggested that the total observed calcium isotope fractionation (~-1.1‰) was larger than that for abiotic calcium isotope fractionation, although calcium isotope fractionation of around -1‰ has been shown to be in range of abiotic carbonate formation (Gussone et al., 2003; Gussone et al., 2005; Gussone et al., 2011; AlKhatib and Eisenhauer, 2017b). The work by Krause et al. (2012) has recently been followed up by further work into microbially induced carbonate precipitation using *Alcanivorax borkumensis*, which displayed a calcium isotope fractionation of -1.19±0.22‰ (Krause et al., 2018).

It remains an open question whether the magnitude of calcium isotope fractionation during microbially-induced carbonate mineral precipitation varies as a function of the growth rate of the carbonate minerals, whether the growth rate of the carbonate minerals varies as a function of bacterial growth rate, or if there are microbially-induced controls on this calcium isotope fractionation factor. Before the calcium isotopic composition of sedimentary carbonate minerals can be used, these controls must be determined. In this study we use pure cultures of a sulfate-reducing bacterium, *Desulfovibrio bizertensis*, in a range of conditions and at a range of culture growth rates to explore the effect that these variable culture growth rates have on the calcium isotope fractionation during microbially-induced carbonate mineral precipitation.

2. Methods

2.1. Culturing of *Desulfovibrio bizertensis*

Culture studies were carried out with *Desulfovibrio bizertensis*, a Gram-negative sulfate-reducing bacteria originally isolated from marine sediments off the coast of Tunisia (Haouari et al., 2006). The strain of *D. bizertensis* used was purchased from Leibniz-Institut Deutche Sammlung von Mikroorganismen und Zellkulturen GmbH (DSMZ). For culture media, Ocean Scientific International Ltd. (OSIL) Atlantic seawater was amended with L-ascorbic acid (0.01% w/v) and Na-thioglycolate (0.01% w/v) as reductants, formate (110 mM) as an electron donor, and resazurin (1 mg/L) as an oxygen indicator. 125 mL of the resulting media was added to each 130 mL culture vial along with 0.3 g kaolinite seeds. The kaolinite seeds were added as potential nucleation sites for the precipitation of calcium carbonate during the growth of the bacteria, although it has previously been shown that kaolinite does not nucleate vaterite (Kralj and Vdović, 2000). Vials were capped with butyl rubber stoppers, crimp sealed, sparged with mixed gas (90% N_2/10% CO_2) for 30 minutes, and autoclaved at 121 ˚C for 90 minutes. Vials were allowed to cool at 25 ˚C, and yeast extract (0.2% w/v) was then added to each vial via syringe filter for additional nutrients.

Bacterial growth was manipulated by the addition of varying concentrations of ampicillin, an antibiotic that inhibits bacterial cell wall synthesis during cell division (Petri, 2011). Ampicillin was chosen because it was reported in the initial isolation of this bacteria that *D. bizertensis* growth could be inhibited by ampicillin at 100 µg/mL (Haouari et al., 2006). In addition, a study of the inhibitory concentrations of varying broad-spectrum antibiotics on a range of human-associated *Desulfovibrio* species observed growth inhibition at ampicillin concentrations ranging from 0.19 – 24 µg/mL, with a concentration that inhibited growth of 50% of isolates (MIC_{50}) of 0.75 µg/mL and a MIC_{90} of 8 µg/mL (Nakao et al., 2009). We reasoned *D. bizertensis* was less likely to be drug resistant than bacterial species found in the human gut, and our goal was to reduce growth rate, not completely inhibit bacterial growth. Cultures were therefore grown with either 0 µg/mL, 0.1 µg/mL, 1 µg/mL, 10 µg/mL, or 100 µg/mL ampicillin in two sets of experiments, in January 2018 and in April 2018. Stock solutions of ampicillin were sparged with nitrogen and then added to culture vials via syringe filter. Vials were inoculated with 1-2 mL of a *D. bizertensis* stock culture and kept under anoxic conditions at 25˚C for the duration of the experiments. For each antibiotic condition, cultures were grown in triplicate, and a negative control was maintained for each

condition. The negative control was inoculated, autoclaved, and then amended with the appropriate volume of yeast extract and ampicillin stock solutions, which would otherwise degrade upon autoclaving.

2.2. Analytical methods

Cultures were sampled immediately after inoculation ("t=0") and then regularly afterwards via needle and syringe, being careful to avoid taking up kaolinite seeds or EPS during sampling. Samples were measured for OD_{600} (optical density at 600 nm), pH, alkalinity, cation and anion concentrations. All UV-Vis spectroscopy used an AquaMate Plus UV-Vis spectrophotometer. Unfiltered media was centrifuged for 5 minutes at 900 rpm to separate any solids before measuring OD_{600} as a proxy for bacterial growth. The remaining sample solution was filtered through a 0.2 μm syringe filter. Solution pH was measured using an Orion 3 Star pH meter with ROSS microelectrode (ORION 8220 BNWP PerpHect ROSS; platinum wire as reference in iodine/potassium solution, with a 3M KCl ROSS internal filling solution). Alkalinity titrations (0.1 M HCl) were performed using a Metrohm 848 Titrino Plus. For cation concentrations, 50 μL of raw filtered media was diluted 20 times into Milli-Q water (18.2 MΩ). Ion concentrations were then measured using high-pressure ion chromatography on a Dionex ICS5000+ with an IonPac CS16 column, using methanesulfonic acid (MSA, 30 mM) as the eluent. For anion concentrations, 50 μL of raw filtered media was diluted 20 times into Milli-Q water (18.2 MΩ), and 20 μL of zinc acetate (20% w/v aq.) was added to fix sulfide. The resulting solutions were centrifuged at 10,000 rpm for 5 minutes, and then the supernatant was transferred via pipette into sample vials for further analysis. Anion concentrations were measured on the Dionex ICS5000+ with an IonPac AS18 column, using potassium hydroxide (KOH, 31 mM) as the eluent. 50 μL of filtered sample solution was diluted into 500 μL of zinc acetate (0.05 M aq.) to fix sulfide for measurement of sulfide concentrations. The resulting solution was reacted in the dark for 40 minutes with diamine reagent (20 μL) (6N HCl with $FeCl_2$ (4% w/v) and N,N-dimethylphenylene diamine sulfate (1.6% w/v)). Solutions were diluted with at least 1 mL Milli-Q water, and absorbance at 670 nm was taken. If necessary, samples were diluted further in order to bring absorbance values between 0.087-0.800.

For each sample, the amount of media necessary to obtain 6 μg of calcium was calculated based on the previously determined calcium concentration. The appropriate volume of each sample was spiked with a 42-48 calcium double spike containing 0.1 equivalents of calcium relative to the sample. Samples that had been spiked were dried at 100˚C, then dissolved into 3 μL of concentrated nitric acid, diluted to 750 μL with Milli-Q water and prepared for column separation. Prior to isotope analysis, calcium needs to be separated from other ions in the media so that pure calcium can be loaded onto filaments and into the mass spectrometer. Calcium was purified using the Dionex ICS5000+ with an IonPac CS16 column and methane sulfonic acid (30 mM) as the eluent. For samples with a relatively high concentration of calcium, collection of the calcium fraction was triggered by the machine's recognition of the calcium peak. However, as calcium concentrations dropped over the course of the incubation/culture experiment through carbonate mineral precipitation, peak recognition failed as the calcium peak became smaller relative to the sodium peak. In these cases, sample collection was time-based, collecting all eluent over the time window when calcium normally elutes. The procedural blank on the Dionex as determined independently by ICP-OES is 96 ng of calcium, when 7 ml of eluent was collected from the Dionex. During the collection of 4.4 μg of calcium using the Dionex, this represents ~2% of the collected calcium. (Bradbury and Turchyn, 2018).

Spiked, purified calcium was acidified with distilled nitric acid and dried at 100˚C. For analysis by mass spectrometry, the resulting nitrate salt was dissolved in 1 μL of nitric acid (2M) and deposited in thirds onto rhenium double filaments. Samples then were dried and phosphoric acid (10% aq., 0.5 μL) was added to filament as an activator. Filaments loaded with a 915B standard were prepared alongside the purified samples. The average of the standards 915B and 915A over the course of the measurements were -0.28±0.12‰ (n=68, 2σ) and -1.02±0.04‰ (n=5, 2σ) relative to BSE. Samples and standards were analyzed on a Triton Plus multicollector thermal ionization mass spectrometer (TIMS). The isotope ratios were iteratively corrected to subtract the double spike and yield the final $\delta^{44}Ca$, which is reported in the supplementary data file relative to both BSE and 915A, and through the rest of the manuscript as a relative

change in fluid $\delta^{44}Ca$ from the initial fluid composition in each vial. The average error on ten duplicates run during the study was 0.05‰ (2σ).

2.3. Method for calculating calcium isotope fractionation

In a closed system the calcium isotope fractionation ($\Delta^{44}Ca_{(s\text{-}f)}$) can be calculated using the equation for Rayleigh fractionation:

$$R_t = R_0 f^{(\alpha-1)}$$

Equation 1

where R_t represents the ratio $^{44}Ca/^{40}Ca$ at time t, R_0 represents the initial ratio of the two calcium isotopes, f is the fraction of the initial calcium remaining in the system and alpha (α) is the fractionation factor. Equation 1 can be rearranged to the following equation so that the slope of the line between $\delta^{44}Ca_f$ and –ln(f) is approximately equal to $\Delta^{44}Ca_{(s\text{-}f)}$ (Eqn. 2, Mariotti et al., 1981).

$$\delta^{44}Ca_t = \delta^{44}Ca_0 + \Delta^{44}Ca_{(s-f)} \times -\ln(f)$$

Equation 2

The visualization of multiple calcium isotope fractionation factors using this method on a single plot is much clearer. The benefits of this approach are shown in Fig. 1.

A Monte Carlo simulation was used to determine the error on the calculated calcium isotope fractionation, which is the gradient of the line. By using the instrumental errors ($\delta^{44}Ca$ = ±0.12‰ 2σ, [Ca] = ±2% 2σ) from each measured point, the simulation generates a new value within a normal distribution centered on the measurements. The best fit line—with an origin intercept—is determined. The simulation is then run one thousand times and the 99th percentile is used to determine the maximum error in the gradient. Fig. 1c displays the utility of this approach using theoretical points from the trend in the calcium isotope fractionation displayed in Fig. 1b; the larger the number of measurements, and the lower the fraction of calcium remaining in the solution, the smaller the error on the calculated calcium isotope fractionation is. The Monte Carlo simulation using 5 theoretical points from the calcite fractionation trend gives both a small error (±0.04‰) and the same value as the original fractionation trend (Fig. 1c).

Whereas the use of only three theoretical points from the aragonite fractionation trend, with only a 50% depletion in calcium, gives a much larger error (±0.17‰).

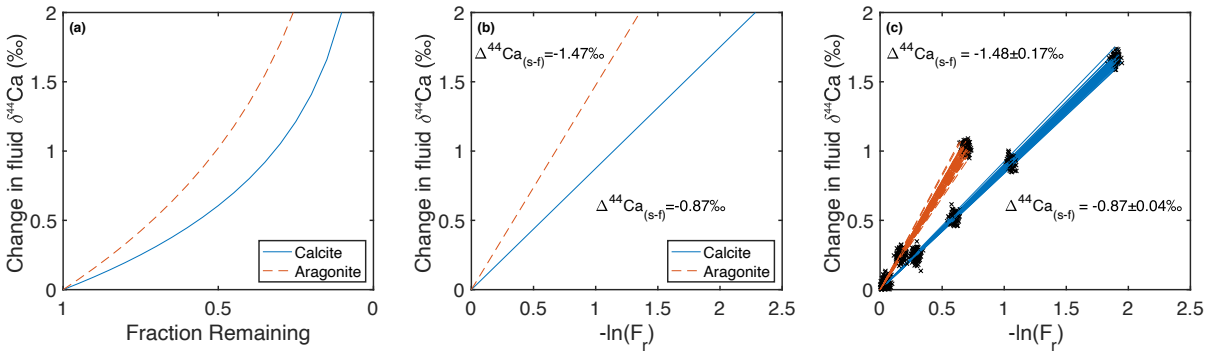

Figure 1: Comparison of two methods of plotting fractionation factors: standard Rayleigh fractionation (a) versus the natural logarithm method (b) using the abiotic aragonite and calcite precipitation trends published in Gussone et al. (2005) given a temperature of 25°C. Panel c demonstrates the utility of a Monte Carlo simulation for determining the error on the calculated calcium isotope fractionation factor (gradient).

3. Results

The pure cultured bacterium *D. bizertensis*, has previously been used to study the precipitation of different calcium carbonate polymorphs under a range of initial solution chemistries in pure culture incubations (Lin et al., 2018). Lin et al., (2018) found that monohydrocalcite was the dominant calcium carbonate polymorph made when the Mg/Ca ratio of the solution was above 2, and calcite was dominantly formed below a Mg/Ca ratio of 2 (Lin et al., 2018). We initially measured the change in the calcium isotopic composition of eight of the cultures in these previously published experiments, exploring the impact that the initial solution chemistry, and hence the carbonate polymorph precipitated, had upon the fractionation of calcium isotopes during carbonate mineral precipitation (Fig. 2). We find that in these experiments, as the calcium concentration decreased, the δ^{44}Ca of the fluid in the vial increased, as the ^{40}Ca was distilled into the carbonate mineral precipitate (monohydrocalcite or calcite), as expected (Fig. 2).

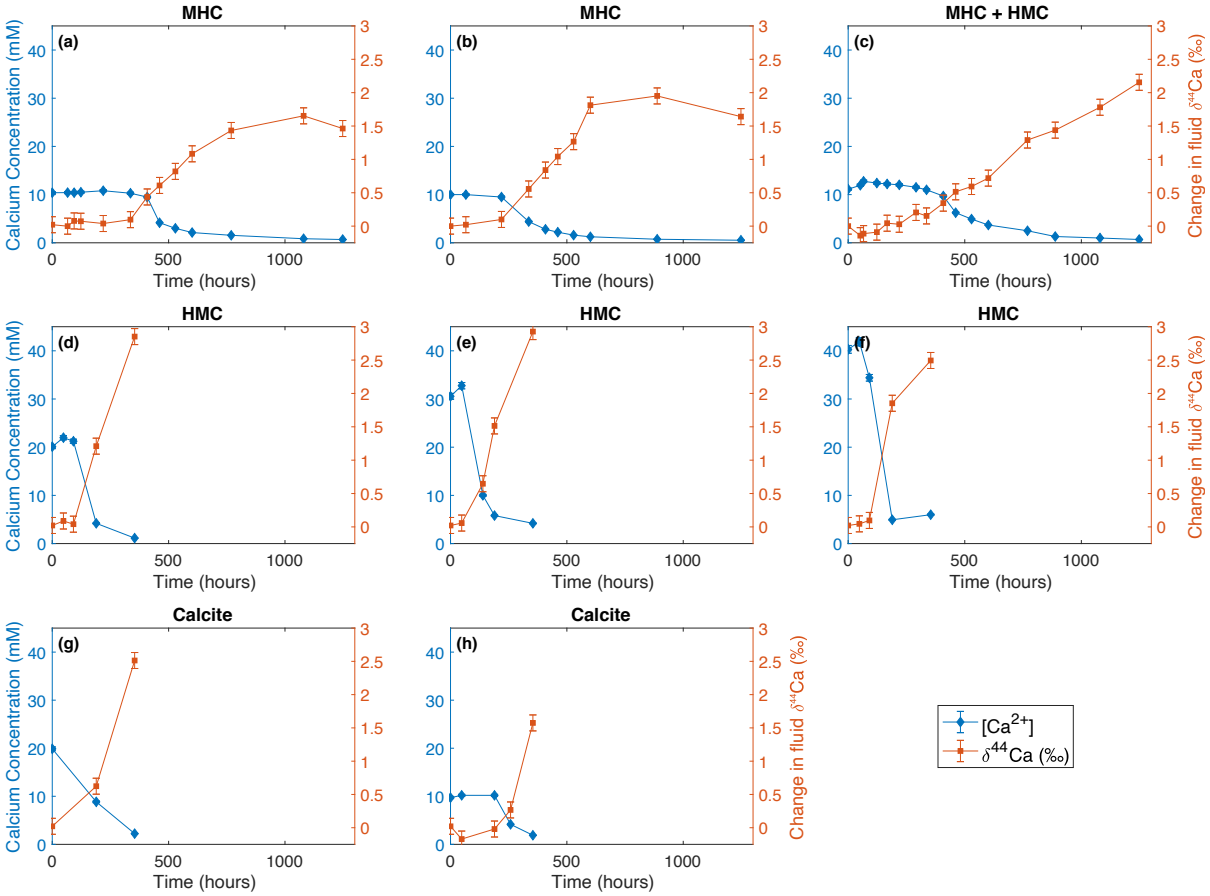

Figure 2: Calcium concentration in solution (blue) and the relative change in calcium isotope composition of the solution (orange) plotted against time of sampling for a range of polymorphs: a,b precipitated monohydrocalcite (MHC), c precipitated monohydrocalcite and magnesian calcite (MHC + HMC), d,e,f precipitated magnesian calcite (HMC), g,h precipitated calcite. The cultures were grown during experiments reported in Lin et al (2018). The error bars on the $\delta^{44}Ca$ are 2σ from the measurement of 915B, and the error bar on the calcium concentration measurements are 2%.

We plot the calcium isotopic composition of the fluid against the natural log of the fraction of calcium remaining within the solution ($-\ln(F_r)$), in order to calculate the fractionation factor as described above (Eqn. 2, Fig. 1). The $\Delta^{44}Ca_{(s\text{-}f)}$ of the experiments varied between -0.56‰ and -1.14‰ (Fig. 3). This is reported as a negative number because the solid has a lower calcium isotope composition relative to the fluid. When monohydrocalcite is the dominant calcium carbonate polymorph, the $\Delta^{44}Ca_{(s\text{-}f)}$ is -0.63 ±0.18‰ (2σ, Fig. 3a); in the experiments where calcite was the dominant calcium carbonate polymorph the $\Delta^{44}Ca_{(s\text{-}f)}$ is -0.95 ±0.41‰ (2σ, Fig. 3c). In some experiments there was a high amount of magnesium in the crystal lattice (as reported in Lin et al., 2018). These high-Mg calcite precipitates have a $\Delta^{44}Ca_{(s\text{-}f)}$ of -1.05 ±0.20‰ (2σ), similar

to the calcite precipitates (Fig. 3b). The calcium isotope fractionation for calcite and high-Mg calcite during microbially-induced carbonate precipitation are both slightly larger than the experimentally determined $\Delta^{44}Ca_{(s\text{-}f)}$ of -0.87‰ at 25°C for abiotic calcite from Gussone et al., (2005), but within a similar range.

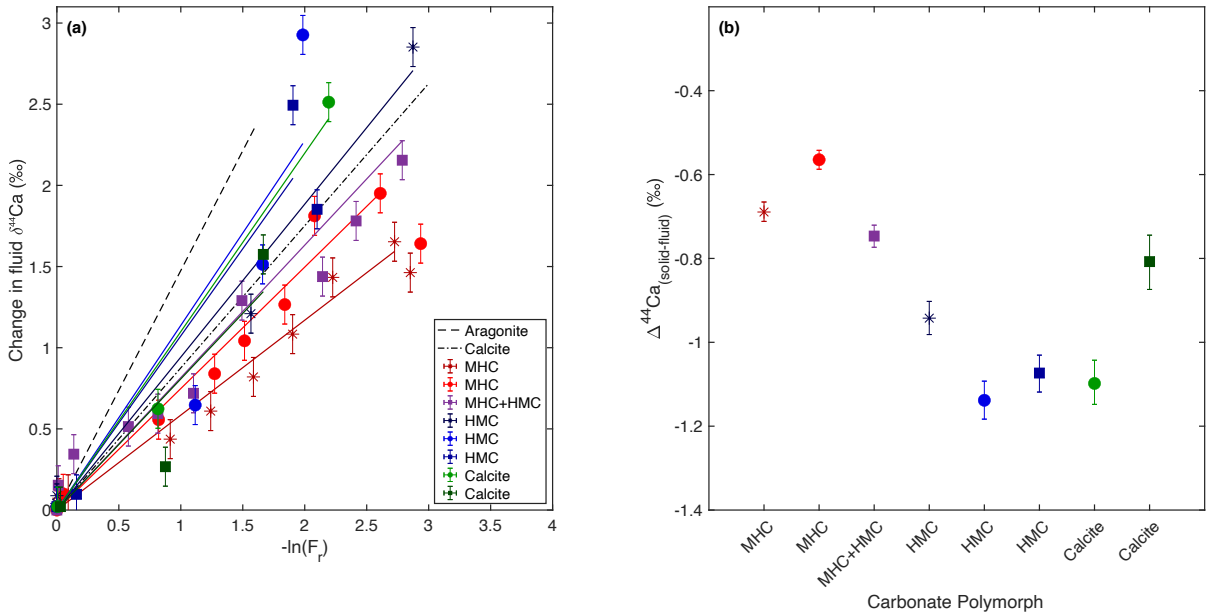

Figure 3: Relative change in calcium isotopic composition versus the negative natural log of the fraction of calcium remaining within the solution, compared to the abiotic aragonite and calcite precipitation trends published in Gussone et al. (2005) given a temperature of 25°C (a). MHC denotes monohydrocalcite and HMC denotes magnesian calcite. Panel b is the calculated $\Delta^{44}Ca_{(s\text{-}f)}$ with the error bars representing the 99th percentile of the slope using a Monte Carlo simulation of the data.

To investigate the impact that changes in the rate of bacterial growth have on the fractionation of calcium isotopes during microbially-induced carbonate mineral precipitation, the initial solution chemistry for the second set of experiments was kept constant to keep the precipitated carbonate polymorph as monohydrocalcite (MHC). Ampicillin was added to the incubations, as described above, which impedes bacterial growth. This is can be observed in the lower maximum OD_{600} of the culture, the slower rates of decrease in sulfate concentrations, and slower rates of increase in alkalinity within the cultures (Fig. 4). Negative controls showed no evidence of bacterial growth over the course of the experiments. The calcium concentration decreases with a

simultaneous increase in the calcium isotopic composition of the media, similar to the first experiments (Fig. 5).

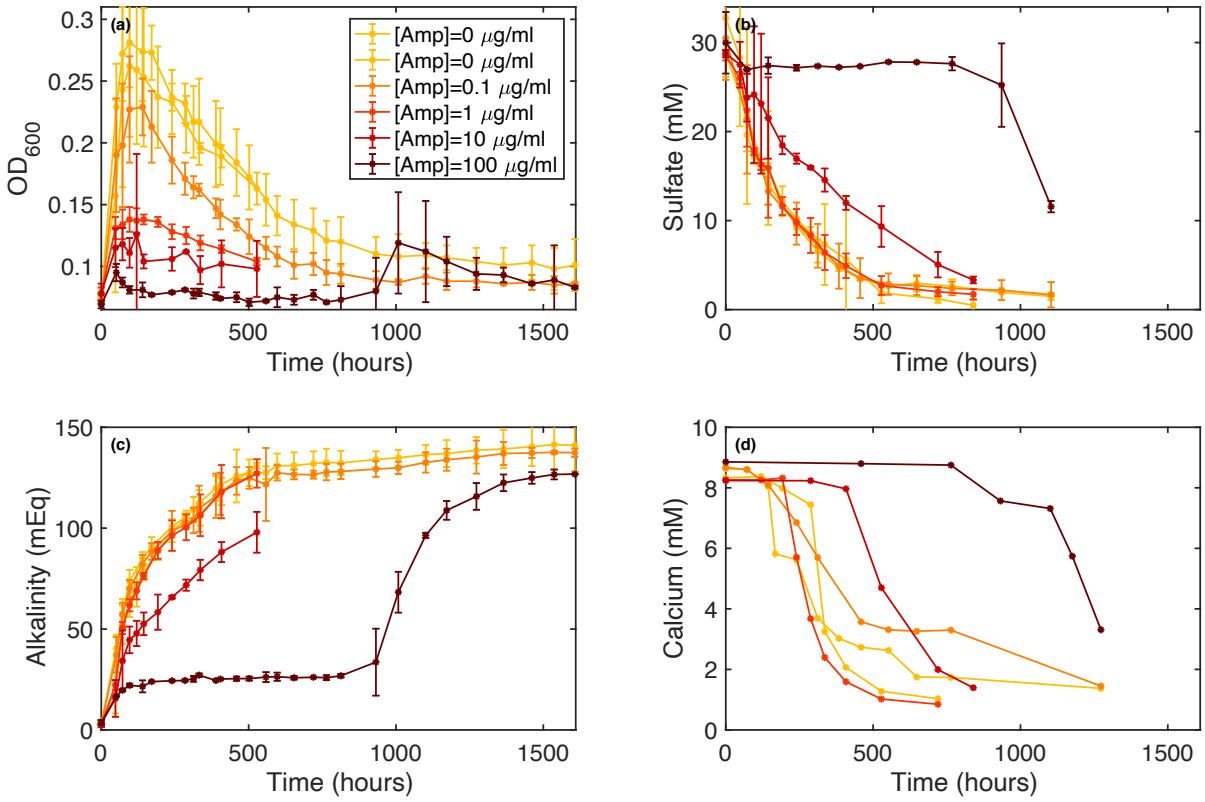

Figure 4: The Optical Density (a), Sulfate concentration (b), Alkalinity (c) and Calcium concentration (d) of the solutions plotted against the time of sampling of the experiments containing ampicillin–0 µg/ml, 0.1 µg/ml, 1 µg/ml, 10 µg/ml or 100 µg/ml. The error bars for OD_{600}, sulfate and alkalinity represent the standard deviation over the three replicates; calcium concentrations were only run on the experiments where calcium isotopes were also run.

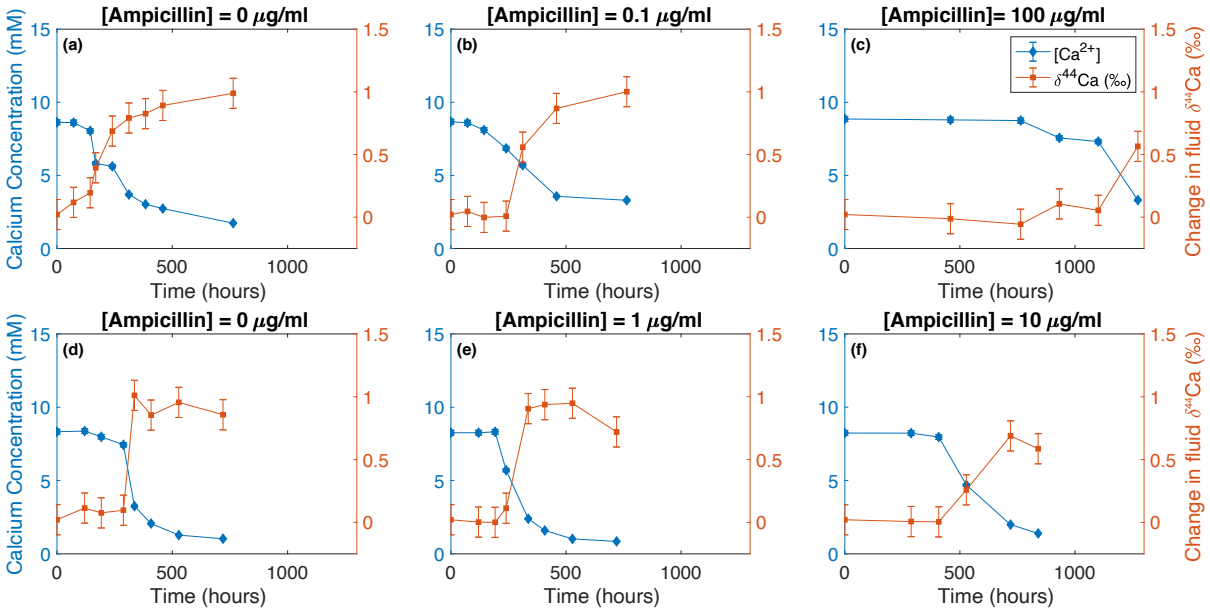

Figure 5: Calcium concentration in solution (blue), and the relative change in calcium isotopes in solution (orange) plotted against time of sampling for ampicillin concentrations ranging from 0 μg/ml (a,d), 0.1 μg/ml (b), 1 μg/ml (e), 10 μg/ml (f) and 100 μg/ml (c). Graphs a-c were measured in the January 2018 set of experiments, whereas d-f were measured in April 2018. The error bars on the $\delta^{44}Ca$ are 2σ from the measurement of 915B, and the error bar on the concentration measurements are 2%.

The earliest—and largest—decreases in calcium concentrations are seen in the samples with the lowest concentrations of ampicillin (0-1 μg/ml), while the time it takes to initiate carbonate mineral precipitation (as seen by the initiation of decrease in calcium concentrations) is later in the experiments with ampicillin concentrations of 10 μg/ml or greater (Fig. 5). The $\Delta^{44}Ca_{(s\text{-}f)}$ of the experiments with varying amounts of ampicillin ranged from -0.48‰ to -1.07‰ (Fig. 6b). In general, the calcium isotope fractionation is larger when the ampicillin concentrations are lower, with the highest calcium isotope fractionation occurring with ampicillin concentrations of 0 and 0.1 μg/ml ($\Delta^{44}Ca_{(s\text{-}f)}$ = -1.04 ±0.09‰, 2σ), and the lowest calcium isotope fractionation occurring with the ampicillin concentrations of 10 and 100 μg/ml ($\Delta^{44}Ca_{(s\text{-}f)}$ = -0.52 ±0.12‰, 2σ). We note that the $\delta^{44}Ca$ diverges from the straight Rayleigh fractionation line soon after initial precipitation is observed; this will be discussed in section 4.3. The calcium isotope fractionation on average in these experiments ($\Delta^{44}Ca_{(s\text{-}f)}$ = -0.88 ±0.42‰, 2σ), is higher than the $\Delta^{44}Ca_{(s\text{-}f)}$ of MHC observed in the initial experiments (-0.63±0.18‰) and highlights the importance of non-mineralogical controls on the calcium isotope fractionation.

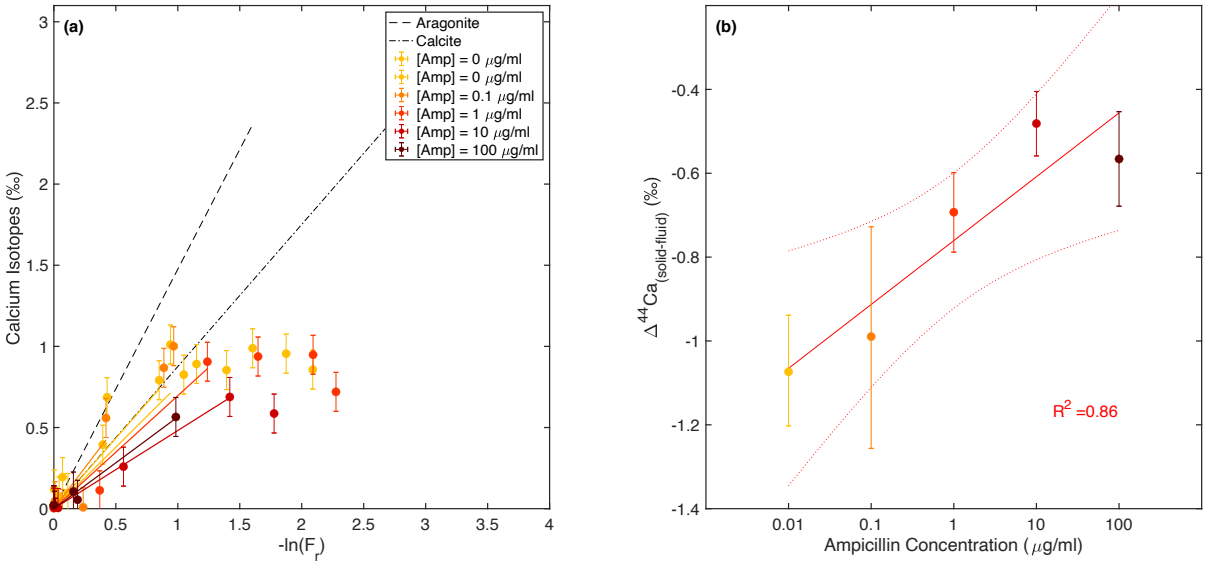

Figure 6: Relative change in calcium isotopes versus the negative natural log of the fraction of calcium remaining within the solution, for ampicillin containing experiments compared to the abiotic aragonite and calcite precipitation trends published in Gussone et al. (2005) given a temperature of 25°C (a). Experiments containing 0.1 µg/ml or lower are displayed in a, 1 µg/ml in b, 10 µg/ml or greater in c, and all ampicillin concentrations are displayed in d. Panel b is the calculated $\Delta^{44}Ca_{(s\text{-}f)}$ with the error bars representing the 99th percentile of the slope using a Monte Carlo simulation of the data. Only the initial points are used to calculate a linear regression for the calcium isotope fractionation and the Monte Carlo simulation, due to the solution reequilibration discussed in Section 4.2. The average of the two solutions with no added ampicillin has been plotted at 0.01 µg/ml to plot on the log scale in panel b.

4. Discussion

4.1. Calcium Isotope Fractionation during microbially induced carbonate precipitation

Several conceptual and numerical models have been proposed to understand the range in calcium isotope fractionation during carbonate mineral precipitation, and its relationship to the rate of mineral precipitation. In one of the most recent models, the calcium isotope fractionation factor of any given carbonate mineral precipitate is taken as the intermediate between the equilibrium calcium isotope fractionation factor (α_{eq}) and the calcium isotope fractionation factor for precipitation at the kinetic limit (α_f), with crystal precipitation and dissolution rates determining the balance (DePaolo,

2011). This model was expanded into an ion-by-ion growth model which allows calcium isotope fractionation to be modelled in terms of solution saturation or the calcium:carbonate ion ratio in solution, where low oversaturation or a high $Ca:CO_3$ ratio is expected to drive calcium isotope fractionation towards the equilibrium limit, and high oversaturation or a low $Ca:CO_3$ ratio will drive calcium isotope fractionation towards the kinetic limit, or larger values (Nielsen et al., 2012). This model was tested in the field at sites with varying calcium concentrations within the same high-alkalinity lake. Larger calcium isotope fractionation was found in locations with lower calcium concentrations (Nielsen and DePaolo, 2013).

In addition to these modeling studies, the majority of laboratory studies exploring calcium isotope fractionation during carbonate mineral precipitation have shown that the faster the rate of mineral growth, the larger the calcium isotope fractionation (e.g. Tang et al., 2008a; AlKhatib and Eisenhauer, 2017b). Experimental studies conducted in sites with slow fluid transport through carbonate systems in both an aquifer and deep-marine sediments have suggested that at equilibrium, the calcium isotope fractionation is close to 0‰ (Fantle and DePaolo, 2007; Jacobson and Holmden, 2008). Microbially-induced calcium carbonate precipitation is neither a biologically precipitated calcium carbonate mineral, where the organism (such as a foraminifera) exerts a high degree of control on the biomineralization, nor an abiotic calcium carbonate, where carbonate minerals are supersaturated and form with no biological control. During growth of the sulfate reducing bacteria *Desulfovibrio bizertensis,* with formate as an electron donor, the bacterial growth increases both the pH and the concentration of bicarbonate ions within the solution. This increases the saturation state for calcium carbonate, whether that is directly or through the precipitation of an amorphous calcium carbonate (ACC) precursor. The bacteria are not physically mediating the mineral growth, and, in some cases, can be entombed by the resultant calcium carbonate precipitation (Lin et al., 2018). However they are influencing the chemistry of the media, and in some cases helping drive carbonate mineral nucleation through the production of EPS (Bosak and Newman, 2003; Braissant et al., 2007; Bontognali et al., 2014).

The calcium isotope fractionation observed during the precipitation of microbially-induced MHC in this study is lower than the calcium isotope fractionation during the

abiotic precipitation of either calcite or aragonite or during the microbially-induced precipitation of calcite and high-Mg calcite (Fig. 3). Indeed, our calculated calcium isotope fractionation factor for MHC is closer to the modelled calcium isotope fractionation factor for carbonate mineral precipitation (-0.6 to -0.7‰, Nielsen et al., 2012). However, the vast majority of carbonate minerals, biotic or abiotic, measured in the natural environment have a larger calcium isotope fractionation between fluid and mineral than suggested by the model in Nielsen et al. (2012). Ultimately MHC will dehydrate and become a more stable calcium carbonate mineral (Kimura and Koga, 2011). Our data hint there may be a two-step calcium isotope fractionation, a smaller partitioning of calcium isotopes during the initial precipitation of MHC, as measured in this study, followed by a second partitioning of calcium isotopes during the transformation of MHC to a more stable calcium carbonate polymorph to produce the larger calcium isotope fractionation often measured in the natural environment in minerals such as calcite, aragonite and high-Mg calcite. Future experiments studying the transformation of MHC to stable calcium carbonate polymorphs may help answer how applicable this study is versus models of abiotic carbonate mineral precipitation.

In the experiments where the growth rate of the bacteria was manipulated using ampicillin, we see a range of calcium isotope fractionation between -0.48 to -1‰ (Fig. 6). The growth rate of the bacteria was estimated using the natural logarithm of the slope of the OD_{600} during the exponential growth phase (Widdel, 2007). The estimated bacterial growth rate correlates with the initial ampicillin concentration of the media (Fig. 7a); this suggests the higher the ampicillin concentration the slower the growth rate of the bacteria. The estimated bacterial growth rate also correlates with the $\Delta^{44}Ca_{(s-f)}$ across all of the incubations, with the slower bacterial growth rates showing lower $\Delta^{44}Ca_{(s-f)}$ values (Fig. 7b).

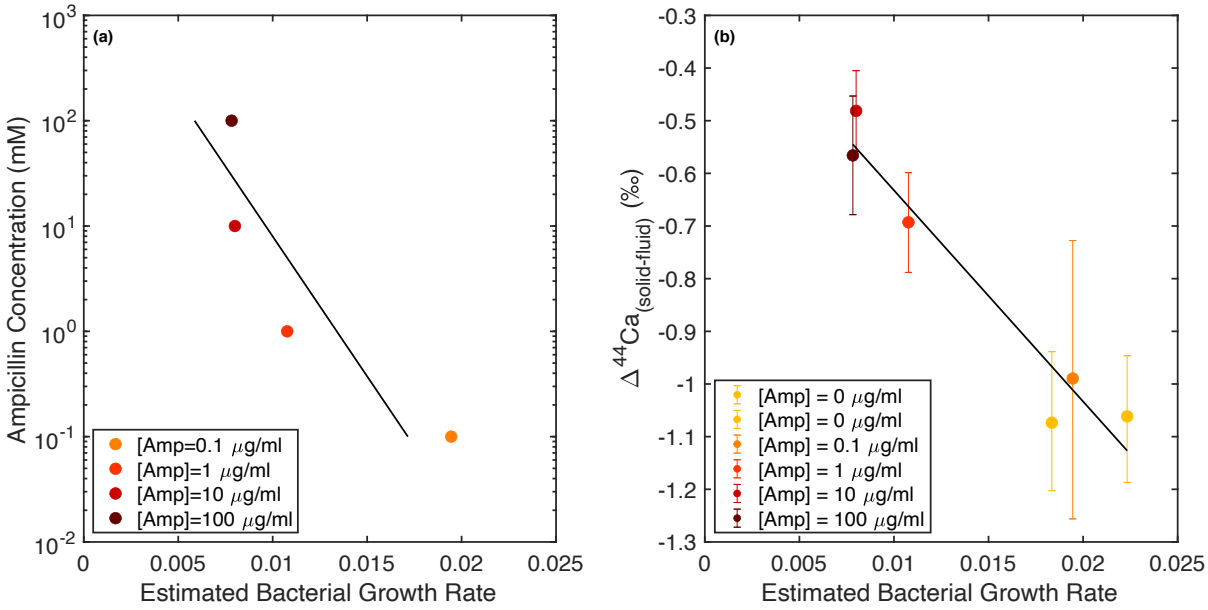

Figure 7: (a) Ampicillin concentration in the solution plot against the maximum OD_{600} slope during culturing (r^2=0.79, p-value<0.01). (b) Bacterial growth rate plotted against the calcium isotope fractionation ($\Delta^{44}Ca_{(s\text{-}f)}$) ($r^2$=0.94, p-value<0.01).

The link we observe between the estimated rate of bacterial growth and the calcium isotope fractionation during carbonate mineral precipitation can also be visualised when we plot the calculated calcium isotope fractionation against the time-to-initial carbonate mineral precipitation and maximum alkalinity during the incubation (Fig. 8).

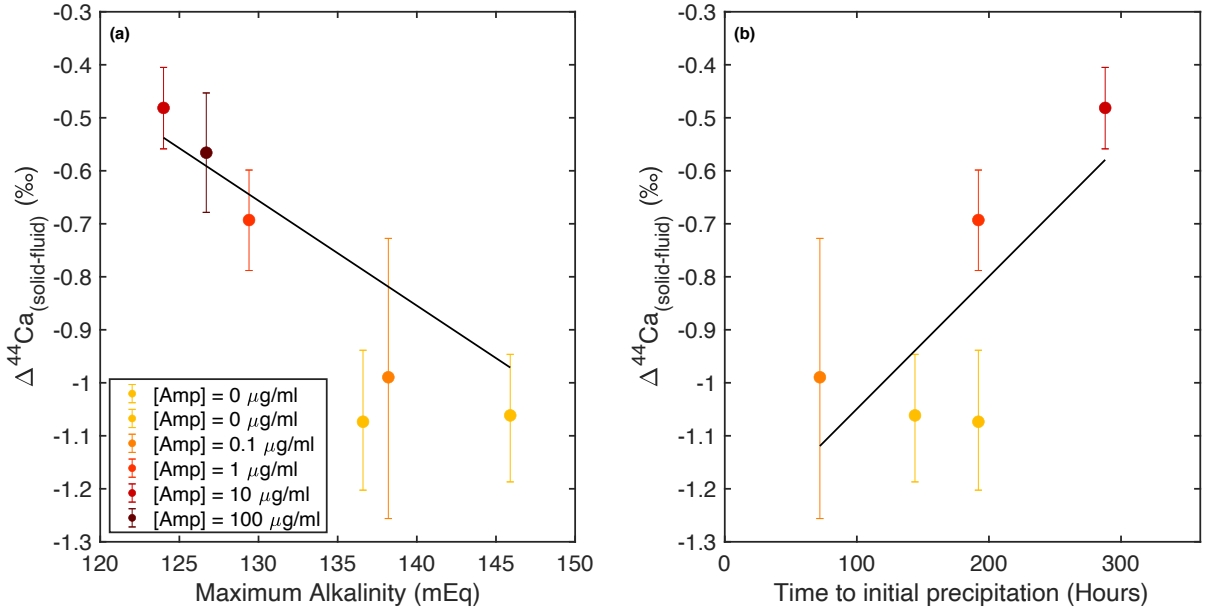

Figure 8: (a) Calcium Isotope fractionation ($\Delta^{44}Ca_{(s\text{-}f)}$) plot against the maximum alkalinity within the solution (r^2=0.71; p-value<0.01). (b) Calcium Isotope fractionation ($\Delta^{44}Ca_{(s\text{-}f)}$) plotted against time to initial precipitation of monohydrocalcite, as evidenced by a decrease in the calcium concentration (r^2=0.55; p-

value=0.05). Magnesian calcite and calcite are included within this plot, as the calcium isotope fractionation appears to follow the same trends as the monohydrocalcite. The experiment with an ampicillin concentration of 100 µg/ml is excluded in (b) as discussed below.

The higher the maximum alkalinity measured in the media, and the shorter the time-to-initial carbonate mineral precipitation in the cultures, the higher the calcium isotope fractionation that we calculate. The bacterial experiments that grow the fastest—and reach the highest maximum alkalinity—create the conditions with the greatest supersaturation with respect to calcium carbonate within the media, driving quicker precipitation of carbonate minerals, in our case monohydrocalcite. This means that precipitation of calcium carbonate occurs the most quickly in the experiments with a high rate of bacterial growth, which leads to the largest calcium isotope fractionation. This suggests the mechanism is similar to abiotic calcium carbonate precipitation as higher mineral growth rates have larger calcium isotope fractionation.

The highest concentration of ampicillin (100 µg/ml) has been excluded in Fig. 8b. In this experiment, over the first 900 hours, the culture acts 'dead' – with no change in optical density (a proxy for cell numbers) or alkalinity (Fig. 4). Then there is, unexpectedly, an increase in both optical density as well as in alkalinity. This delayed growth could be explained in two ways. Ampicillin is inherently unstable over time, and increasingly so at pH>7; at 25°C, ampicillin has been reported to decrease to 80% of its initial potency within 5 days (Gallelli, 1967). The initial high concentration of ampicillin is likely to have inhibited bacterial growth, and as the ampicillin degraded, the bacteria began to grow. An alternative is that the use of ampicillin provides a selective pressure that reduces competition for, and favors selection of, bacteria with ampicillin resistance. Both of these hypotheses suggest that the later phase of growth is not related to the initial growth rate of the *Desulfovibrio bizertensis,* and hence, the calcium isotope fractionation does not correlate with the time taken for precipitation to occur in the 100 µg/mL incubation.

4.2. Rate of mineral precipitation

Ideally, we'd like to link our calcium isotope fractionation to the rate of carbonate mineral precipitation in the incubation vials. In previous studies, when the rate of

precipitation of carbonate minerals has been related to the calcium isotope fractionation factor, the data have been reported in terms of micromoles of carbonate precipitated per unit surface area per time (R in μmol m^{-2} s^{-1}) (Tang et al., 2008a; Nielsen et al., 2012; Harouaka et al., 2014). The rate of carbonate mineral precipitation (R) are typically calculated using the following equation (Tang et al., 2008b):

$$R = \frac{M}{S * t}$$

Equation 3

where M (mmol) is the decrease in aqueous calcium concentration, t is time (hours), and S is the total reactive surface area. We can calculate the reaction rate for our cultures without ampicillin as both M and t are known from our experiments, but we need to estimate the total reactive surface area (S). This is challenging in our experimental setup, as both kaolinite seeds and EPS can act as nucleation sites for the precipitation of calcium carbonate minerals (Aloisi et al., 2006; Tourney and Ngwenya, 2009). We have used four methods to estimate the reactive surface area, and then compare our rate of carbonate mineral precipitation versus calcium isotope fractionation with the data in Tang et al., 2008a for each method. The first method for estimating the reactive surface area is to use the surface area from the kaolinite seeds of 4.3 m^2 (14.3121 m^2/g, Fig. 9a). The second was to use the average reactive surface area from Tang et al. (2008b) of 0.081 m^2 (0.27 m^2/g, Fig. 9b). If we take an inverse approach, the best fit of our data with the data from Tang et al. (2008b) is achieved with a reactive surface area of 0.075 m^2 (0.25 m^2/g, Fig. 9c). Finally, we use a reactive surface area estimate calculated with the time dependent regression equation from Tang et al. (2008b) which is displayed in Fig. 9d.

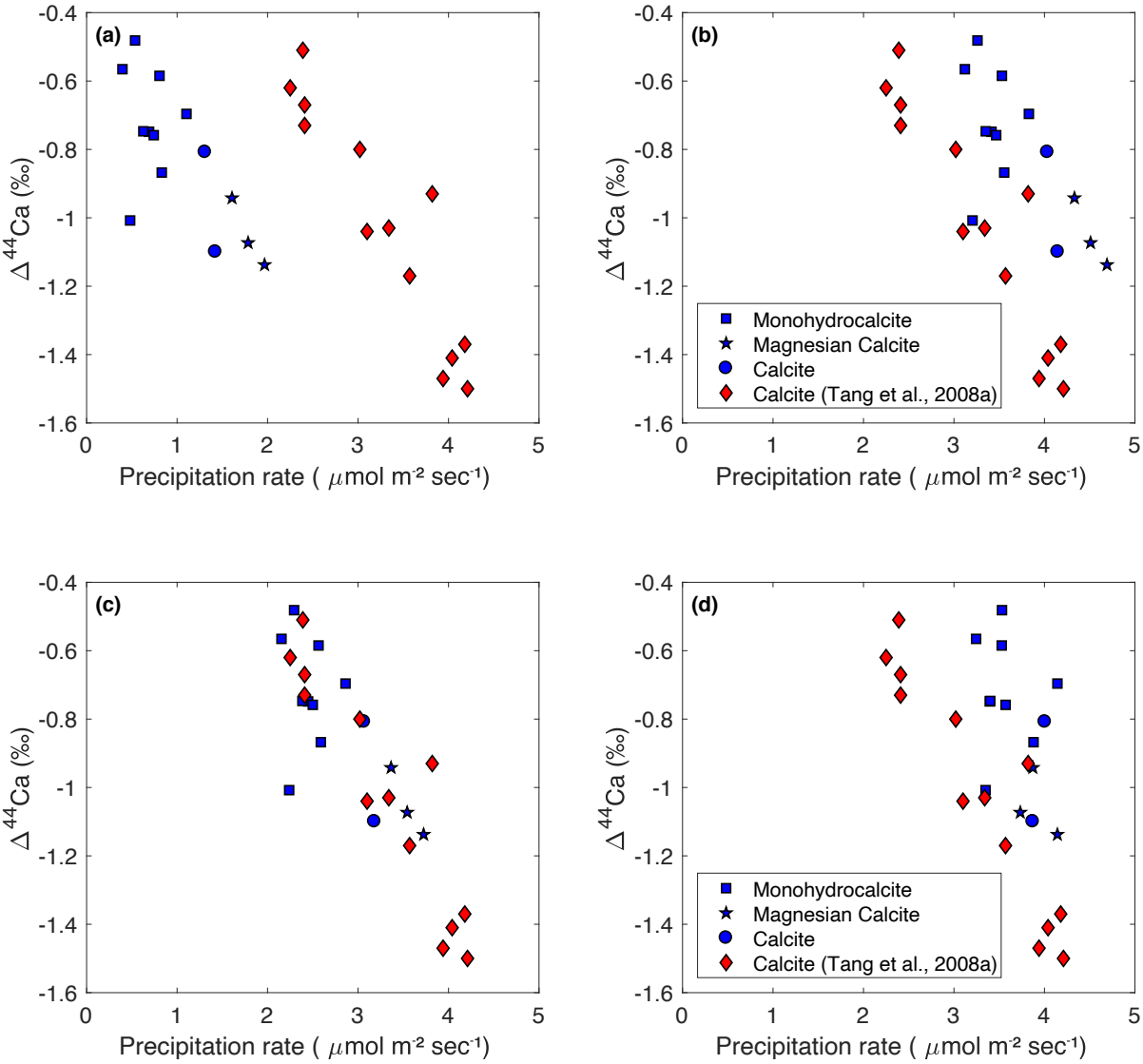

Figure 9: Precipitation rate of the carbonate minerals plotted against the fractionation. Data from this study are blue, whereas previously published data are red (Tang et al., 2008a). The four panels show four methods of estimating the reactive surface area in order to calculate the precipitation rate. Panel a, b and c have constant reactive surface areas of 4.3, 0.0056 and 0.075 m respectively. Panel d had variable reactive surface area based on precipitating calcite following the approach of Tang et al., (2008b).

Our data suggest that using the surface area from kaolinite alone gives the weakest fit for expected relationship between the precipitation of MHC and the calcium isotope fractionation compared to the previously published data (Fig. 9a). The best-fit surface area approximation of 0.25 m^2/g suggests that either the MHC is precipitating on <2% of the surface area of the Kaolinite seeds (potentially at edge or corner sites), or that the nucleation is occurring on the EPS or bacteria themselves. This is similar to the conclusion of Lin et al., (2018), where the microbially-induced carbonate minerals were shown to be precipitating around cells rather than on the mineral seeds in the incubation vials.

585 **4.3. Modelling the calcium isotope back reaction**

586

587 In five of our fourteen experiments, the $\delta^{44}Ca_{fluid}$ stays constant or decreases in the last
588 few time points analysed, while the calcium concentrations continue to decrease (Fig.
589 6). In a simple Rayleigh-style model (Fig. 1), decreasing calcium concentrations in a
590 closed system should drive the calcium isotope composition in the fluid to higher
591 values, and there should be no decrease in the fluid $\delta^{44}Ca$. This decrease in the $\delta^{44}Ca$ at
592 the latter stages of the growth experiments could be linked to a 'back reaction' between
593 the precipitated calcium carbonate minerals, with their lower $\delta^{44}Ca$, and the residual
594 fluid in the media. During this exchange the ^{40}Ca-enriched solid isotopically
595 reequilibrates with the media, lowering the $\delta^{44}Ca$ in the media. Because the calcium
596 concentration in the fluid continues to decrease, this back reaction must be through
597 recrystallisation; recrystallisation suggests a rate of precipitation that matches or barely
598 exceeds a rate of dissolution. By comparing the difference between the predicted
599 $\delta^{44}Ca_{fluid}$ and the measured $\delta^{44}Ca_{fluid}$, the rate of this recrystallisation can be quantified.

600

601 There are a couple of key assumptions that need to be made in order to model this rate
602 of recrystallisation. First, we assume that there is no calcium isotope fractionation
603 during dissolution. This assumption has previously been used in modelling carbonate
604 recrystallisation rates (Fantle and DePaolo, 2007; Fantle, 2015; Gorski and Fantle, 2017;
605 Bradbury and Turchyn, 2018), although recent work has suggested it may not always be
606 the case (Oelkers et al., 2019). Second, we assume that the dissolving solid has the same
607 calcium isotopic composition as the carbonate minerals that precipitated earlier in the
608 experiment. Finally, we assume either that the calcium isotope fractionation during
609 precipitation is the same as that during the initial precipitating calcium carbonate
610 (calculated from the Rayleigh fractionation models of the initial points), or that there is
611 no calcium isotope fractionation on precipitation, a quasi-equilibrium condition (Fantle
612 and DePaolo, 2007; Fantle, 2015; Huber et al., 2017).

613

614 With these assumptions, a simple box model can be created, where we track the time
615 dependent change in the mass of calcium in the fluid (M_{Ca}) towards the end of the
616 experiments:

$$\frac{dM_{Ca}}{dt} = F_{Ca_{dis}} - F_{Ca_{ppt}}$$

Equation 4

where F_{Ca} represents the flux of calcium into and out of the fluid through dissolution (*dis*) and precipitation (*ppt*) respectively. Thus, the mass of calcium in the fluid at any time point is a function of the dissolution and precipitation fluxes. The calcium isotopic composition of the fluid can then be tracked alongside this calcium mass balance by the addition of terms for the isotopic composition of the fluid ($\delta^{44}Ca_{fluid}$) and solid ($\delta^{44}Ca_{solid}$) at the previous time point (t-1), and a term for the calcium isotopic fractionation during precipitation ($\Delta^{44}Ca_{ppt}$) (Equation 2):

$$\delta^{44}Ca_{fluid_t} = \frac{M_{Ca_{t-1}} * \delta^{44}Ca_{fluid_{t-1}} + F_{Ca_{dis}} * \delta^{44}Ca_{solid_{t-1}} - F_{Ca_{ppt}} * (\delta^{44}Ca_{fluid_{t-1}} - \Delta^{44}Ca_{ppt})}{M_{Ca_t}}$$

Equation 5

By substituting equation 4 into equation 5 we can calculate the mass of calcium that is dissolving and precipitating, as other variables are known. The mass of calcium we calculate that is supplied to the solution from carbonate mineral dissolution can be compared to the total mass of calcium in the solution to get the percentage of the solid that is exchanging per day, which is a recrystallisation rate. We do this for the case where there is calcium isotope fractionation on precipitation and for the case where there is no calcium isotope fractionation on precipitation (Fig. 10).

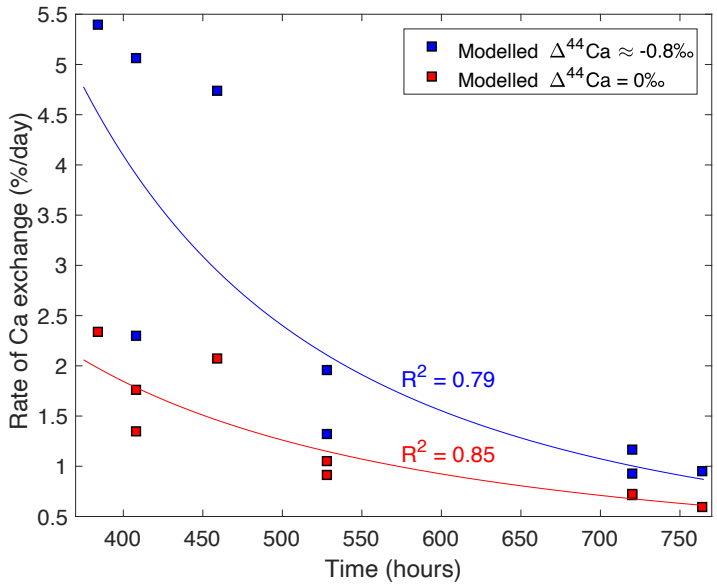

Figure 10: The modelled rate of calcium exchange between the solid and the fluid in percent per day plotted against the time of sampling. The two colours represent the two conflicting calcium isotope fractionation scenarios: red represents 'equilibrium' fractionation ($\Delta^{44}Ca_{ppt}$ = 0‰), and blue represents 'kinetic' fractionation that is the same as the initial calcium isotope fractionation on microbially-induced carbonate mineral precipitation ($\Delta^{44}Ca_{ppt}$ ~ -0.8‰). The best-fit lines follow a power law, with both relationships being statistically significant ($p<0.05$).

This calculation suggests that the exchange of calcium between the newly precipitated MHC and the fluid occurs most rapidly immediately after precipitation, and the rate of exchange decreases with time, with increasing deviation from the Rayleigh fractionation trend being observed as the calcium concentrations continue to decrease over the course of the experiments. The decrease in overall rate of recrystallisation has previously been suggested in other recrystallising systems, and is thought to be due to the increasing stability of minerals over time, the mechanism behind which is still debated (White et al., 1996; Curti et al., 2010; Avrahamov et al., 2013; Gorski and Fantle, 2017).

These observations show that while calcium isotope fractionation during microbially induced MHC precipitation is dependent on variability in bacterial growth, the interpretation of these signals in the geological record will be extremely challenging due to the need to better understand the calcium isotope fractionation during the transformation of MHC to more stable calcium carbonate minerals. Observations will be further complicated by potential changes in $\delta^{44}Ca$ during the dehydration of MHC to a more stable phase. Further work is required to see if similar bacteria growth rate dependence is found in more stable carbonate polymorphs, and whether this could then

be observed in the geological record. The final observation is that the range in calcium isotope fractionation observed within these simple bacterial experiments matches or exceeds the variability of calcium isotopes used to explore many major geological events such as the End Permian Mass extinction (0.3‰) and End-Triassic mass extinction (0.8‰) (Payne et al., 2010; Jost et al., 2017), which shows the importance of further research into the impact of bacteria on the calcium isotope signature recorded in sedimentary carbonate cements.

5. Conclusions

In this study we report new measurements of the calcium isotope fractionation in bacterially induced carbonate growth, which are similar to previously determined calcium isotope fractionation values during abiotic precipitation. Bacterial growth rate is correlated with the calcium isotope fractionation of the monohydrocalcite that precipitates, with faster bacterial growth rates leading to precipitates with a higher calcium isotope fractionation. The mechanism for the control of bacterial growth rate on calcium isotope fractionation is proposed to be through solution supersaturation and hence carbonate precipitation rate. The comparison of the rate of carbonate precipitation with previously published data provides further evidence that monohydrocalcite is precipitating around the EPS or the bacteria themselves relative to the kaolinite seeds.

The bacterially induced monohydrocalcite was unstable with respect to calcium isotopes and showed a rapid exchange between the solid and the fluid. This observation suggests that the calcium isotope signal recorded may not be linked to the original precipitation rates over long time scales. The rate of exchange decreases with time, potentially leaving a calcium isotope signature preserved in the MHC that is a balance between the amount of exchange and the original fractionation. The exchange and the low initial calcium isotope fractionation factors suggest that bacterially induced carbonate might be relatively similar in $\delta^{44}Ca$ to the fluid it precipitated from.

693 The combination of these insights helps to constrain the impact that bacteria can have
694 on precipitated calcium carbonate, and direct future work into area of calcium isotope
695 fractionation during bacterially induced carbonate precipitation.
696
697 ## 6. Acknowledgments
698
699 The work was supported by ERC 307582 StG (CARBONSINK) to AVT and NERC
700 NE/R013519/1 to HJB.
701
702
703 ## 7. References
704
705 Ahm A.-S. C., Bjerrum C. J., Blättler C. L., Swart P. K. and Higgins J. A. (2018) Quantifying
706 early marine diagenesis in shallow-water carbonate sediments. *Geochimica et*
707 *Cosmochimica Acta* **236**, 140–159.

708 Ahm A.-S. C., Maloof A. C., Macdonald F. A., Hoffman P. F., Bjerrum C. J., Bold U., Rose C.
709 V., Strauss J. V. and Higgins J. A. (2019) An early diagenetic deglacial origin for
710 basal Ediacaran "cap dolostones." *Earth and Planetary Science Letters* **506**, 292–
711 307.

712 AlKhatib M. and Eisenhauer A. (2017a) Calcium and strontium isotope fractionation
713 during precipitation from aqueous solutions as a function of temperature and
714 reaction rate; II. Aragonite. *Geochimica et Cosmochimica Acta* **209**, 320–342.

715 AlKhatib M. and Eisenhauer A. (2017b) Calcium and strontium isotope fractionation in
716 aqueous solutions as a function of temperature and reaction rate; I. Calcite.
717 *Geochimica et Cosmochimica Acta* **209**, 296–319.

718 Aloisi G., Gloter A., Krüger M., Wallmann K., Guyot F. and Zuddas P. (2006) Nucleation of
719 calcium carbonate on bacterial nanoglobules. *Geology* **34**, 1017–1020.

720 Avrahamov N., Sivan O., Yechieli Y. and Lazar B. (2013) Carbon isotope exchange during
721 calcite interaction with brine: implications for 14C dating of hypersaline
722 groundwater. *Radiocarbon* **55**, 81–101.

723 Berner R. A. (2003) The long-term carbon cycle, fossil fuels and atmospheric
724 composition. *Nature* **426**, 323–326.

725 Berner R. A., Lasaga A. C. and Garrels R. M. (1983) Carbonate-silicate geochemical cycle
726 and its effect on atmospheric carbon dioxide over the past 100 million years. *Am.*
727 *J. Sci.; (United States)* **283:7**. Available at: https://www.osti.gov/biblio/6582171
728 [Accessed August 23, 2018].

729 Bontognali T. R. R., McKenzie J. A., Warthmann R. J. and Vasconcelos C. (2014)
730 Microbially influenced formation of Mg-calcite and Ca-dolomite in the presence

731 of exopolymeric substances produced by sulphate-reducing bacteria. *Terra Nova*
732 **26**, 72–77.

733 Bosak T. and Newman D. K. (2003) Microbial nucleation of calcium carbonate in the
734 Precambrian. *Geology* **31**, 577–580.

735 Bradbury H. J. and Turchyn A. V. (2018) Calcium isotope fractionation in sedimentary
736 pore fluids from ODP Leg 175: Resolving carbonate recrystallization. *Geochimica*
737 *et Cosmochimica Acta* **236**, 121–139.

738 Braissant O., Decho A. W., Dupraz C., Glunk C., Przekop K. M. and Visscher P. T. (2007)
739 Exopolymeric substances of sulfate-reducing bacteria: Interactions with calcium
740 at alkaline pH and implication for formation of carbonate minerals. *Geobiology* **5**,
741 401–411.

742 Curti E., Fujiwara K., Iijima K., Tits J., Cuesta C., Kitamura A., Glaus M. A. and Müller W.
743 (2010) Radium uptake during barite recrystallization at 23±2°C as a function of
744 solution composition: An experimental 133Ba and 226Ra tracer study.
745 *Geochimica et Cosmochimica Acta* **74**, 3553–3570.

746 De La Rocha C. L. and DePaolo D. J. (2000) Isotopic evidence for variations in the marine
747 calcium cycle over the cenozoic. *Science* **289**, 1176–8.

748 DePaolo D. J. (2011) Surface kinetic model for isotopic and trace element fractionation
749 during precipitation of calcite from aqueous solutions. *Geochimica et*
750 *Cosmochimica Acta* **75**, 1039–1056.

751 Druhan J. L., Steefel C. I., Williams K. H. and DePaolo D. J. (2013) Calcium isotope
752 fractionation in groundwater: Molecular scale processes influencing field scale
753 behavior. *Geochimica et Cosmochimica Acta* **119**, 93–116.

754 Du Vivier A. D. C., Jacobson A. D., Lehn G. O., Selby D., Hurtgen M. T. and Sageman B. B.
755 (2015) Ca isotope stratigraphy across the Cenomanian–Turonian OAE 2: Links
756 between volcanism, seawater geochemistry, and the carbonate fractionation
757 factor. *Earth and Planetary Science Letters* **416**, 121–131.

758 Fantle M. S. (2015) Calcium isotopic evidence for rapid recrystallization of bulk marine
759 carbonates and implications for geochemical proxies. *Geochimica et*
760 *Cosmochimica Acta* **148**, 378–401.

761 Fantle M. S. and DePaolo D. J. (2007) Ca isotopes in carbonate sediment and pore fluid
762 from ODP Site 807A: The Ca2+(aq)–calcite equilibrium fractionation factor and
763 calcite recrystallization rates in Pleistocene sediments. *Geochimica et*
764 *Cosmochimica Acta* **71**, 2524–2546.

765 Fantle M. S. and DePaolo D. J. (2005) Variations in the marine Ca cycle over the past 20
766 million years. *Earth and Planetary Science Letters* **237**, 102–117.

767 Fantle M. S. and Tipper E. T. (2014) Calcium isotopes in the global biogeochemical Ca
768 cycle: Implications for development of a Ca isotope proxy. *Earth-Science Reviews*
769 **129**, 148–177.

Farkaš J., Frýda J. and Holmden C. (2016) Calcium isotope constraints on the marine carbon cycle and CaCO3 deposition during the late Silurian (Ludfordian) positive δ13C excursion. *Earth and Planetary Science Letters* **451**, 31–40.

Gallelli J. F. (1967) Stability Studies of Drugs Used in Intravenous Solutions: Part One. *Am J Hosp Pharm* **24**, 424–433.

Garrels R. M. and Lerman A. (1981) Phanerozoic cycles of sedimentary carbon and sulfur. *PNAS* **78**, 4652–4656.

Gorski C. A. and Fantle M. S. (2017) Stable mineral recrystallization in low temperature aqueous systems: A critical review. *Geochimica et Cosmochimica Acta* **198**, 439–465.

Gussone N., Böhm F., Eisenhauer A., Dietzel M., Heuser A., Teichert B. M. A., Reitner J., Wörheide G. and Dullo W.-C. (2005) Calcium isotope fractionation in calcite and aragonite. *Geochimica et Cosmochimica Acta* **69**, 4485–4494.

Gussone N., Eisenhauer A., Heuser A., Dietzel M., Bock B., Böhm F., Spero H. J., Lea D. W., Bijma J. and Nägler T. F. (2003) Model for kinetic effects on calcium isotope fractionation (δ44Ca) in inorganic aragonite and cultured planktonic foraminifera. *Geochimica et Cosmochimica Acta* **67**, 1375–1382.

Gussone N., Nehrke G. and Teichert B. M. A. (2011) Calcium isotope fractionation in ikaite and vaterite. *Chemical Geology* **285**, 194–202.

Haouari O., Fardeau M.-L., Casalot L., Tholozan J.-L., Hamdi M. and Ollivier B. (2006) Isolation of sulfate-reducing bacteria from Tunisian marine sediments and description of Desulfovibrio bizertensis sp. nov. *Int J Syst Evol Microbiol* **56**, 2909–2913.

Harouaka K., Eisenhauer A. and Fantle M. S. (2014) Experimental investigation of Ca isotopic fractionation during abiotic gypsum precipitation. *Geochimica et Cosmochimica Acta* **129**, 157–176.

Hein J. R., O'neil J. R. and Jones M. G. (1979) Origin of authigenic carbonates in sediment from the deep Bering Sea. *Sedimentology* **26**, 681–705.

Henderson G. M., Chu N.-C., Bayon G. and Benoit M. (2006) δ44/42 Ca in gas hydrates, porewaters and authigenic carbonates from Niger Delta sediments. *Geochimica et Cosmochimica Acta Supplement* **70**, A244–A244.

Higgins J. A., Blättler C. L., Lundstrom E. A., Santiago-Ramos D. P., Akhtar A. A., Crüger Ahm A.-S., Bialik O., Holmden C., Bradbury H., Murray S. T. and Swart P. K. (2018) Mineralogy, early marine diagenesis, and the chemistry of shallow-water carbonate sediments. *Geochimica et Cosmochimica Acta* **220**, 512–534.

Huber C., Druhan J. L. and Fantle M. S. (2017) Perspectives on geochemical proxies: The impact of model and parameter selection on the quantification of carbonate recrystallization rates. *Geochimica et Cosmochimica Acta* **217**, 171–192.

Husson J. M., Higgins J. A., Maloof A. C. and Schoene B. (2015) Ca and Mg isotope constraints on the origin of Earth's deepest C excursion. *Geochimica et Cosmochimica Acta* **160**, 243–266.

Jacobson A. D. and Holmden C. (2008) δ44Ca evolution in a carbonate aquifer and its bearing on the equilibrium isotope fractionation factor for calcite. *Earth and Planetary Science Letters* **270**, 349–353.

Jost A. B., Bachan A., Schootbrugge B. van de, Brown S. T., DePaolo D. J. and Payne J. L. (2017) Additive effects of acidification and mineralogy on calcium isotopes in Triassic/Jurassic boundary limestones. *Geochemistry, Geophysics, Geosystems* **18**, 113–124.

Kimura T. and Koga N. (2011) Thermal Dehydration of Monohydrocalcite: Overall Kinetics and Physico-geometrical Mechanisms. *J. Phys. Chem. A* **115**, 10491–10501.

Kozdon R., Kelly D. C. and Valley J. W. (2018) Diagenetic Attenuation of Carbon Isotope Excursion Recorded by Planktic Foraminifers During the Paleocene-Eocene Thermal Maximum. *Paleoceanography and Paleoclimatology* **33**, 367–380.

Kralj D. and Vdović N. (2000) The influence of some naturally occurring minerals on the precipitation of calcium carbonate polymorphs. *Water Research* **34**, 179–184.

Krause S., Liebetrau V., Gorb S., Sánchez-Román M., McKenzie J. A. and Treude T. (2012) Microbial nucleation of Mg-rich dolomite in exopolymeric substances under anoxic modern seawater salinity: New insight into an old enigma. *Geology* **40**, 587–590.

Krause S., Liebetrau V., Löscher C. R., Böhm F., Gorb S., Eisenhauer A. and Treude T. (2018) Marine ammonification and carbonic anhydrase activity induce rapid calcium carbonate precipitation. *Geochimica et Cosmochimica Acta* **243**, 116–132.

Kump L. R. and Arthur M. A. (1999) Interpreting carbon-isotope excursions: carbonates and organic matter. *Chemical Geology* **161**, 181–198.

Lau K. V., Maher K., Brown S. T., Jost A. B., Altıner D., DePaolo D. J., Eisenhauer A., Kelley B. M., Lehrmann D. J., Paytan A., Yu M., Silva-Tamayo J. C. and Payne J. L. (2017) The influence of seawater carbonate chemistry, mineralogy, and diagenesis on calcium isotope variations in Lower-Middle Triassic carbonate rocks. *Chemical Geology* **471**, 13–37.

Lein A. Y. (2004) Authigenic Carbonate Formation in the Ocean. *Lithology and Mineral Resources* **39**, 1–30.

Lin C. Y., Turchyn A. V., Steiner Z., Bots P., Lampronti G. I. and Tosca N. J. (2018) The role of microbial sulfate reduction in calcium carbonate polymorph selection. *Geochimica et Cosmochimica Acta* **237**, 184–204.

Linzmeier B. J., Jacobson A. D., Sageman B. B., Hurtgen M. T., Ankney M. E., Petersen S. V., Tobin T. S., Kitch G. D. and Wang J. (2019) Calcium isotope evidence for environmental variability before and across the Cretaceous-Paleogene mass extinction. *Geology*. Available at: https://pubs.geoscienceworld.org/gsa/geology/article/574630/Calcium-isotope-evidence-for-environmental [Accessed December 11, 2019].

Mariotti A., Germon J. C., Hubert P., Kaiser P., Letolle R., Tardieux A. and Tardieux P. (1981) Experimental determination of nitrogen kinetic isotope fractionation: Some principles; illustration for the denitrification and nitrification processes. *Plant Soil* **62**, 413–430.

Milliman J. D. (1993) Production and accumulation of calcium carbonate in the ocean: Budget of a nonsteady state. *Global Biogeochem. Cycles* **7**, 927–957.

Nakao K., Tanaka K., Ichiishi S., Mikamo H., Shibata T. and Watanabe K. (2009) Susceptibilities of 23 Desulfovibrio Isolates from Humans. *Antimicrobial Agents and Chemotherapy* **53**, 5308–5311.

Nielsen L. C. and DePaolo D. J. (2013) Ca isotope fractionation in a high-alkalinity lake system: Mono Lake, California. *Geochimica et Cosmochimica Acta* **118**, 276–294.

Nielsen L. C., DePaolo D. J. and De Yoreo J. J. (2012) Self-consistent ion-by-ion growth model for kinetic isotopic fractionation during calcite precipitation. *Geochimica et Cosmochimica Acta* **86**, 166–181.

Oelkers E. H., Pogge von Strandmann P. A. E. and Mavromatis V. (2019) The rapid resetting of the Ca isotopic signatures of calcite at ambient temperature during its congruent dissolution, precipitation, and at equilibrium. *Chemical Geology* **512**, 1–10.

Payne J. L., Turchyn A. V., Paytan A., DePaolo D. J., Lehrmann D. J., Yu M. and Wei J. (2010) Calcium isotope constraints on the end-Permian mass extinction. *PNAS* **107**, 8543–8548.

Petri W. A. (2011) Penicillins, cephalosporins, and other β-lactam antibiotics. *Goodman and Gilman: The pharmacological basis of therapeutics, Brunton LL, Chabner BA, and Knollmann BB (ed. s), 12th edition, McGraw Hill Medical*, 1477–1505.

Schrag D. P., Higgins J. A., Macdonald F. A. and Johnston D. T. (2013) Authigenic Carbonate and the History of the Global Carbon Cycle. *Science* **339**, 540–543.

Skulan J., DePaolo D. J. and Owens T. L. (1997) Biological control of calcium isotopic abundances in the global calcium cycle. *Geochimica et Cosmochimica Acta* **61**, 2505–2510.

Tang J., Dietzel M., Böhm F., Köhler S. J. and Eisenhauer A. (2008a) Sr2+/Ca2+ and 44Ca/40Ca fractionation during inorganic calcite formation: II. Ca isotopes. *Geochimica et Cosmochimica Acta* **72**, 3733–3745.

884 Tang J., Köhler S. J. and Dietzel M. (2008b) Sr2+/Ca2+ and 44Ca/40Ca fractionation
885 during inorganic calcite formation: I. Sr incorporation. *Geochimica et*
886 *Cosmochimica Acta* **72**, 3718–3732.

887 Teichert B. M. A., Gussone N., Eisenhauer A. and Bohrmann G. (2005) Clathrites:
888 Archives of near-seafloor pore-fluid evolution (δ44/40Ca, δ13C, δ18O) in gas
889 hydrate environments. *Geology* **33**, 213–216.

890 Teichert B. M. A., Gussone N. and Torres M. E. (2009) Controls on calcium isotope
891 fractionation in sedimentary porewaters. *Earth and Planetary Science Letters*
892 **279**, 373–382.

893 Tourney J. and Ngwenya B. T. (2009) Bacterial extracellular polymeric substances (EPS)
894 mediate CaCO3 morphology and polymorphism. *Chemical Geology* **262**, 138–146.

895 Wang S., Yan W., Magalhães H. V., Chen Z., Pinheiro M. L. and Gussone N. (2012) Calcium
896 isotope fractionation and its controlling factors over authigenic carbonates in the
897 cold seeps of the northern South China Sea. *Chin. Sci. Bull.* **57**, 1325–1332.

898 White A. F., Blum A. E., Schulz M. S., Bullen T. D., Harden J. W. and Peterson M. L. (1996)
899 Chemical weathering rates of a soil chronosequence on granitic alluvium: I.
900 Quantification of mineralogical and surface area changes and calculation of
901 primary silicate reaction rates. *Geochimica et Cosmochimica Acta* **60**, 2533–2550.

902 Widdel F. (2007) Theory and measurement of bacterial growth. *Di dalam*
903 *Grundpraktikum Mikrobiologie* **4**, 1–11.

904 Zhu P. and Macdougall J. D. (1998) Calcium isotopes in the marine environment and the
905 oceanic calcium cycle. *Geochimica et Cosmochimica Acta* **62**, 1691–1698.

906